Proceedings of the 21st ICSMGE, Vienna, Austria, 14 – 19 June 2026. Pistrol, Adam & Schweiger (eds.)
Published by: ÖGG, Austrian Society for Geomechanics, Salzburg, Austria, ISBN 978-3-9503898-4-5
https://doi.org/10.53243/ICSMGE2026-2343

Effect of water content of sandy soils on erosion resistance characteristics

Taketo Sato and Hideharu Sugimoto
Structure Technology division, Railway Technical Research Institute, Tokyo, Japan, sato.taketo.67@rtri.or.jp

ABSTRACT: The evaluation method for erosion failure of embankments has not yet been adequately established. One of the reasons is that the erosion resistance of embankment materials is considered to vary with water content, although the details of this relationship remain unclear. This study experimentally investigates the effects of soil moisture conditions on the erosion resistance of embankment materials. Erosion tests were conducted using specimens with identical dry density but varying initial water content to examine the influence of moisture conditions on erosion resistance. In addition, model overflow experiments were performed under a constant initial water content, while varying infiltration conditions, such as water ponding and artificial rainfall. The erosion tests revealed that erosion behavior changed depending on the flow velocity. Under low-velocity conditions, soil particle detachment was dominant, and erosion resistance was primarily governed by the weight of individual particles. In contrast, at high flow velocities, clod detachment was more prevalent, indicating that shear strength was the dominant factor in erosion resistance. When specimens were not immersed, erosion resistance increased with higher initial water content at the time of compaction. However, under water-immersed conditions, the influence of initial water content was found to be negligible, likely due to the development of pore water pressure, which reduced effective stress and consequently lowered shear strength. Model overflow experiments demonstrated that higher water levels, induced by prior ponding, led to significant increases in erosion. On the other hand, under low water level conditions, where pore water pressure was limited, erosion was less severe. Furthermore, rainfall infiltration increased the degree of saturation but had only a minor effect on erosion extent unless it also raised the water level. These results suggest that water pressure plays a more critical role than the degree of saturation alone.

KEYWORDS: Erosion, infiltration, overflow.

1 INTRODUCTION

In recent years, extreme weather events have become increasingly frequent due to the impacts of climate change, and their frequency and intensity are projected to rise further in the future. In Japan, several failures in railway embankments have been attributed to rainfall. These failures include seepage-induced collapse, erosion, scouring, and subsidence. In engineering practice, stability assessments against rainfall-induced failures often focus on seepage failure; however, evaluation methods employing physical models for surface erosion failure remain underdeveloped. One reason for this is the insufficient understanding of the mechanisms governing erosion resistance in geotechnical materials.

Unlike riverbed scouring, surface erosion on embankment slopes typically occurs under unsaturated conditions, with moisture content varying over time due to rainfall infiltration. Previous overflow experiments on levees (Mizutani et al., 2013) showed that pre-saturation increased erosion, suggesting that rainfall and surface water infiltration strongly influence erosion behavior. However, limited research has addressed how the moisture conditions of geotechnical materials affect their erosion resistance. Understanding this relationship is essential for improving the assessment of embankment stability under rainfall events.

Based on the above background, this study experimentally evaluated the influence of infiltration on the erosion resistance characteristics of embankment materials. Specifically, erosion tests were conducted by varying the initial water content and the presence or absence of water immersion, in order to quantitatively assess their effects on erosion resistance. In addition, model overflow experiments were performed under different conditions of immersion water and simulated rainfall to evaluate the degree of erosion in response to infiltration.

2 OVERVIEW OF EROSION TEST METHOD

2.1 *Testing apparatus*

An erosion testing apparatus was constructed based on apreviously developed setup (Briaud et al. 1999). An overview of the apparatus is shown in Figure 1. The system comprises two water tanks, two submersible pumps, an open-channel flume, and a specimen-holding fixture. By operating up to two submersible pumps, each with a discharge capacity of 0.1 m^3/min, water can be circulated from the downstream tank to the upstream tank. This circulation system allows for the execution of long-duration erosion tests.

The internal dimensions of the open channel flume are 3000 mm in length, 200 mm in width, and 190 mm in height. A specimen mold is installed 750 mm from the downstream end along the horizontal direction on the bottom of the flume. The mold has an oval cross-section with internal dimensions of 140

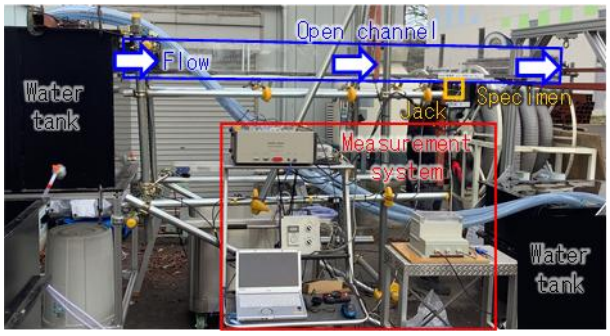

(a) External view.

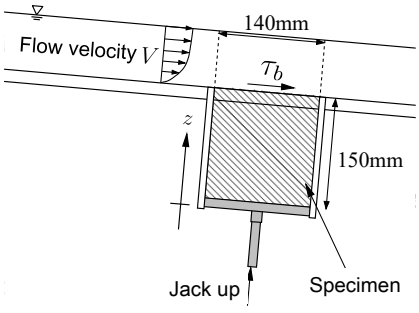

(b) Schematic diagram near the specimen.

Figure 1. Overview of the Erosion Testing Apparatus.

mm in width, 70 mm in depth, and 150 mm in height. A screw jack is attached to the bottom of the mold, allowing for the vertical displacement of the specimen at a maximum rate of 1.1 mm/s. During erosion failure of the specimen, the screw jack is controlled to maintain the specimen's top surface flush with the flume bottom, and the jack's upward displacement speed is interpreted as the erosion rate of the specimen.

The flow velocity in the open channel can be adjusted by altering the number of operating pumps and the slope angle of the flume.

2.2 *Test materials*

The test material used in this study was Inagi sand, which is commonly employed in actual construction of residential and railway embankments. The primary material properties of Inagi sand are listed in Table 1. Inagi sand is classified as silty sand (S-F) in JGS soil classification, characterized by the sand content S_c of 86.2%, the fines content F_c of 12.1 %, and the uniformity coefficient U_c of 5.2, indicating a predominance of relatively uniform sand particles with minor fine content.

According to the compaction test based on JIS A 0432:2020 (Method A-c), the maximum dry density ρ_{dmax} was found to be 1.721 g/cm³ and the optimum water content w_{opt} was 16.2 %. The results of the compaction test are shown in Figure 2.

2.3 *Test cases*

An overview of the test cases is presented in Table 2, and the specimen preparation conditions plotted on the compaction curve are illustrated in Figure 2. In this study, test specimens were prepared with the target dry density of ρ_d = 1.635 g/cm³, the degree of compaction D_c of 95 %. The initial water contents w_{ini} of the specimens were set at 12.2 %, 16.2%, and 19.2 %, and the effects on erosion resistance were compared. Since it was difficult to control the degree of saturation through infiltration during testing, specimens were prepared with the desired initial moisture content instead. Additionally, erosion resistance was also evaluated for specimens constructed at various initial water contents and then subjected to increased degrees of saturation through prolonged soaking. For each condition, erosion tests were conducted under flow velocities ranging from 0.5 to 1.2 m/s.

2.4 *Test procedure*

In each test, after constructing the specimen in the mold within the apparatus, the submersible pumps were operated to circulate water from the downstream to the upstream tank, thereby creating flow in the open channel and reproducing erosion failure on the upper surface of the specimen.

For test cases involving water immersion, water was applied to the top surface of the specimen, followed by a 40-minute resting period before initiating the erosion test. During the test, after confirming that the specimen's top surface was level with the flume bottom, the flow velocity was measured using an electromagnetic flowmeter.

Erosion failure was simulated by circulating water through the open channel using submersible pumps, either after specimen preparation or after increasing the specimen's degree of saturation. The flow velocity was adjusted by varying the number of pumps in operation and the slope of the flume, which was set at a maximum of 1.0° from the horizontal.

Upon confirmation of erosion failure, the screw jack speed was adjusted so that the top surface of the specimen remained level with the flume bottom, allowing the jack's upward speed to be interpreted as the erosion rate. The flatness between the specimen surface and the flume bottom was confirmed visually and verified using a laser displacement sensor (Model: IL-600,

Table 1. Summary of material properties of Inagi sand.

		Inagi sand
JGS soil cassification	-	S-F
Soil particle density ρ_s	g/cm^3	2.721
Maximum dry density ρ_{dmax}	g/cm^3	1.721
Optimum water content w_{opt}	%	16.2
Gravel fraction content G_c	%	1.7
Sand fraction content S_c	%	86.2
Fine fraction content F_c	%	12.1
Maximum diameter D_{max}	mm	9.5

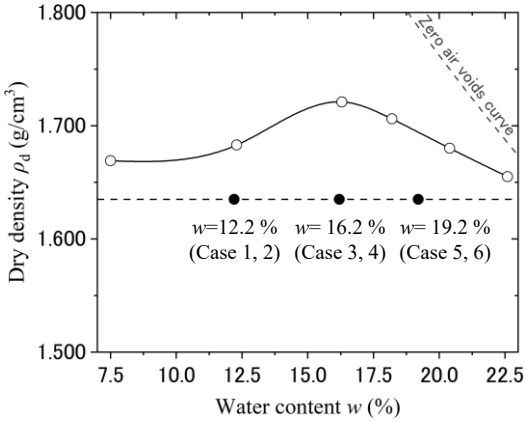

Figure 2. Specimen preparation conditions on the compaction curve.

Table 2. List of test cases.

	Initial water content w_{ini} (%)	Water immersing	Flow velocity v (m/s)	Number of tests
Case 1	12.2	Absent	0.50-0.73	7
Case 2	12.2	Present	0.50-0.80	8
Case 3	16.2	Absent	0.45-1.21	9
Case 4	16.2	Present	0.50-0.73	7
Case 5	19.2	Absent	0.50-1.21	8
Case 6	19.2	Present	0.48-0.85	8

Keyence Corporation). The flow velocity in the flume was then measured using an electromagnetic flowmeter. Each combination of conditions was tested 7–9 times with varying flow velocities.

3 RESULT OF EROSION TESTS

3.1 *Erosion failure modes*

In all test cases, it was observed that the erosion mode varied depending on the applied flow velocity. Among the cases, Case 4 provided the clearest visual documentation of the test conditions; thus, the discussion of erosion failure modes will focus on this representative case. The erosion behavior of the specimen is shown in Figure 3. At a flow velocity of 0.50 m/s (Figure 3. (a), turbidity in the downstream water was observed, and the erosion mainly involved the outflow of soil particle and small soil aggregates. In contrast, at 0.55 m/s (Figure 3. (b), prominent detachment of visible soil chunks was observed, and the downstream flow exhibited significantly increased turbidity due to the disintegration of these chunks and the outflow of finer particles.

This dependence of erosion mode on flow velocity is consistent with findings by Nishimori et al. (2009), who reported similar behavior in their closed-flume experiments. They conducted image-based analysis of the erosion process in saturated cohesive soils and identified two dominant modes: mist-like elution under low shear stress and clod-like detachment under higher shear stress conditions.

Although a silty sand was used in the present study, the erosion behavior observed was consistent with the trends

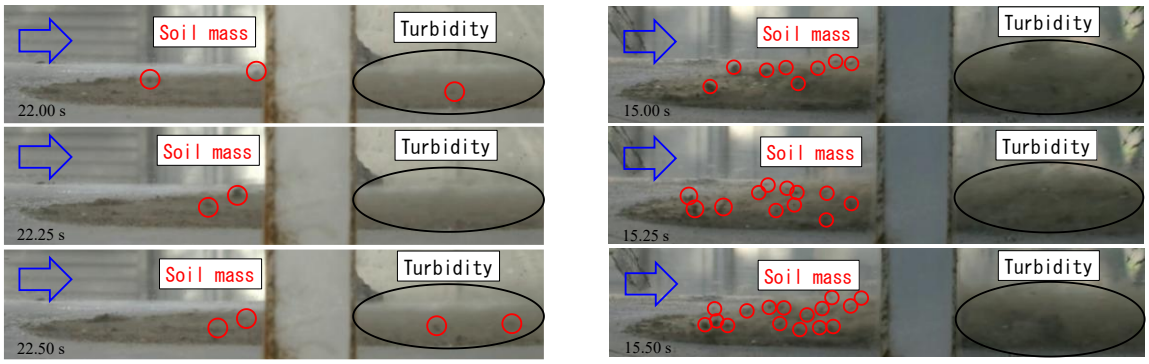

(a) Flow velocity 0.50 m/s. (b) Flow velocity0.55 m/s.

Figure 3. Erosion failure behavior of the specimen in the representative case (Case 4).

reported for cohesive soils by Nishimori et al. (2009).

3.2 *Influence of initial water content on erosion resistance*

Figure 4 presents the relationship between erosion rate and flow velocity for specimens with different initial water contents, excluding those subjected to water immersion. The critical flow velocity is defined here as the threshold at which erosion begins. As confirmed earlier, under low flow velocities, erosion primarily involves the outflow of particles and small aggregates, where particle weight is the main resisting factor. Thus, changes in initial water content had limited influence on erosion rates, and the critical flow velocities were generally similar.

On the other hand, under high flow velocities where erosion is dominated by chunk detachment, the shear strength of the soil becomes the primary resisting factor. Lower initial water contents were associated with higher erosion rates at a given flow velocity. This is attributed to variations in the amount of infiltrated water during testing, which is discussed further in the next section.

3.3 *Influence of water immersion on erosion resistance*

The effect of infiltration water on the erosion resistance characteristics of the specimens is discussed in this section. Figure 5 shows the relationship between erosion rate and flow velocity for cases that considered water immersion. When specimens were subjected to water immersion, their erosion resistance characteristics were generally similar regardless of initial water content.

Additionally, as shown in Figure 4, for specimens with an initial water content w_{ini} of 12.2%, erosion resistance remained similar regardless of water immersion. In contrast, for w_{ini} values of 16.2% and 19.2%, the erosion rate under low flow velocity conditions remained nearly constant, regardless of immersion. However, under high flow velocity conditions, water immersion caused a noticeable increase in the slope of the erosion rate–flow velocity relationship, indicating a greater susceptibility to erosion failure.

As previously discussed, under low flow velocity conditions, soil particle weight is the dominant resistance factor, which may explain why water immersion had a minimal effect. In contrast, at high flow velocities, shear strength governs erosion resistance. It is therefore presumed that water immersion induces pore water pressure, reducing effective stress and thereby lowering erosion resistance.

Fujisawa et al. (2008) reported that the critical shear stress at which erosion initiates remains largely constant across different dry densities. However, under elevated shear stress, erosion rates were lower for specimens with higher dry densities. This implies that higher shear strength associated with higher dry density enhances erosion resistance, consistent with the present findings under high flow conditions.

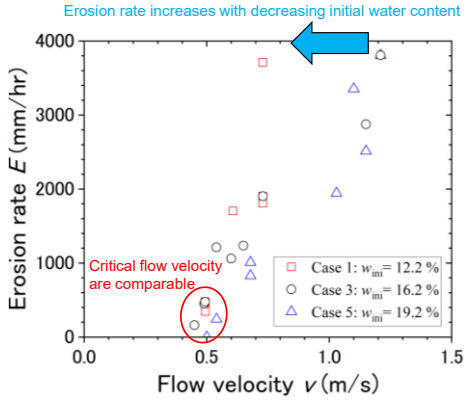

Figure 4. Relationship between erosion rate and flow velocity under different initial water contents without water immersion.

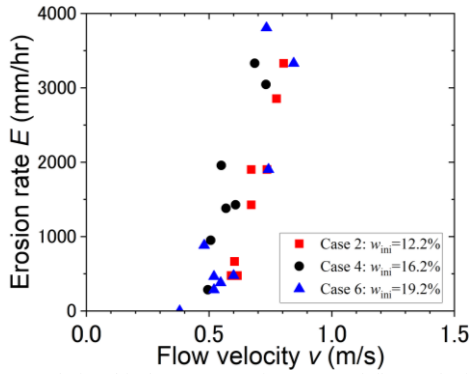

Figure 5. Relationship between erosion rate and flow velocity under different initial water contents with water immersion.

For the initial water content w_{ini} of 12.2%, water immersion had little effect on erosion resistance. In contrast, for the initial water content w_{ini} of 16.2% and 19.2%, immersion resulted in a clear reduction in resistance. This difference is likely due to variations in permeability: specimens with lower initial water content exhibited higher infiltration capacity, allowing surface water to permeate more effectively during the erosion test—even in the absence of pre-immersion. As a result, unsaturated specimens with the initial water content w_{ini} of 12.2% may have exhibited erosion resistance comparable to that of immersed specimens. In contrast, the initial water content w_{ini} of 16.2 % specimens experienced moderate infiltration effects, while those with the initial water content w_{ini} of 19.2 % showed only minimal infiltration, making them more susceptible to strength loss under immersion.

The relationship between initial water content and infiltration rate has been previously addressed in the literature.

Wei et al. (2022) observed that, in rainfall experiments using loam soils, lower initial water content resulted in higher infiltration rates, based on measurements from soil moisture sensors installed at multiple depths. Philip (1969) theoretically demonstrated that higher initial volumetric moisture content leads to reduced sorptivity—a key indicator of capillarity—and lower cumulative infiltration.

Thus, the specimens with lower initial water content may have exhibited similar erosion resistance to saturated specimens due to their higher infiltration capacity during testing. In contrast, specimens with higher initial moisture content experienced reduced resistance due to the development of pore water pressure and the resulting loss of shear strength.

4 OVERVIEW OF THE MODEL OVERFLOW EXPERIMENTS

Table 3 lists the experimental cases of the model overflow tests. A total of four cases were conducted, varying the model scale and the infiltration conditions prior to overflow. Cases 1 and 2 utilized the erosion testing apparatus, while Cases 3 and 4 employed the overflow testing apparatus developed by Watanabe et al (2020), as detailed in their publication.

Figure 6 illustrates the configuration of the embankment models used in each case. In Cases 1 and 2, a model scale of 1:40 relative to the prototype was assumed, and embankment models with a height of 0.1 m were used. These cases aimed to evaluate the effect of upstream water level formation on erosion intensity. Prior to overflow testing, water was retained up to the crest on the upstream side of the embankment model, with or without a standing period to allow for infiltration. The overflow tests were then conducted using a submersible pump with a flow rate of 0.1 m³/min.

In Cases 3 and 4, a model scale of 1:10 was assumed, and embankment models with a height of 0.4 m were used. These cases were designed to simulate conditions where a water level in the embankment does not fully develop, in order to assess the influence of the degree of saturation on erosion intensity. To vary the degree of saturation distribution within the embankment, rainfall simulation was applied or omitted depending on the case. Rainfall was simulated at an average intensity of 15.6 mm/h for a duration of 205 minutes, resulting in a cumulative rainfall of 53.3 mm. This was followed by a 150-minute resting period, after which the overflow test was conducted using a submersible pump with a flow rate of 0.6 m³/min.

Table 3. List of model overflow experiment cases.

	Model height (mm)	Ponding water	Rainfall splinking	Overflow rate (m^3/min)
Case 1	100	Absent	Absent	0.1
Case 2	100	Present	Absent	0.1
Case 3	400	Absent	Absent	0.6
Case 4	400	Absent	Present	0.6

In all cases, the embankment models were constructed using Inagi sand (classified as silty sand, S-F), which was also used in the erosion tests. The target compaction conditions were a dry density ρ_d of 1.635 g/cm³ (corresponding to the degree of compaction D_c of 95.0 %) and an initial water content w_{ini} of 16.2 %.

5 RESULTS AND DISCUSSION OF THE MODEL OVERFLOW EXPERIMENTS

5.1 *Influence of Water Level on the Degree of Erosion*

The assumed water level in the embankment model for Case 2 is shown in Figure 6(a). Under the condition of standing water, seepage was observed from the downstream toe of the slope. Considering the extended standing time prior to the test, an estimated water line was drawn in the figure, connecting the upstream water level and the seepage point. This suggests that the water level was formed throughout most of the embankment body.

The erosion conditions at 10 seconds after the start of the overflow experiments for Cases 1 and 2 are shown in Figure 7, and schematic cross-sectional sketches at the glass surface are presented in Figure 8. When standing water was applied, a tendency for increased erosion near the mid-slope region was observed. As shown in Figures 4 and 5, water immersion of the embankment material appeared to reduce erosion resistance, resulting in increased erosion volume.

Previous studies have similarly reported that pre-saturation of embankment models prior to overflow leads to increased erosion, and this trend was confirmed in the present study as well. These findings are consistent with the decrease in erosion

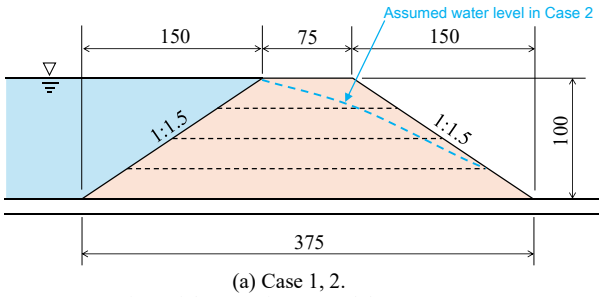

(a) Case 1, 2.

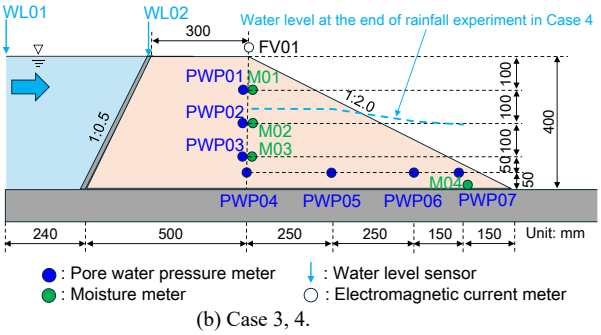

(b) Case 3, 4.

Figure 6. Overview of the experiment models.

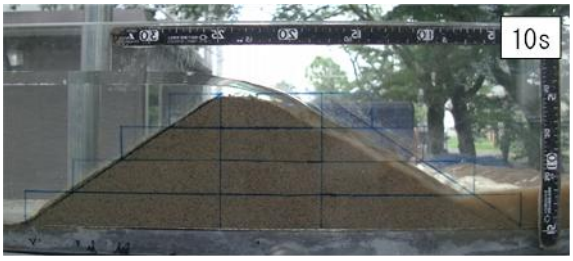

(a) Case 1 Non-ponded condition.

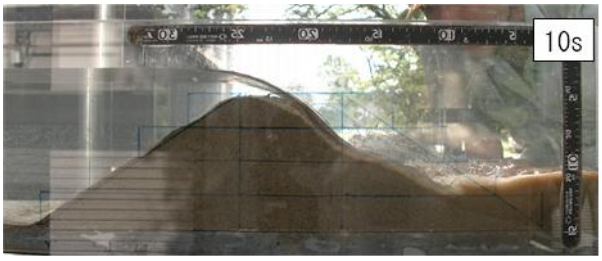

(b) Case 2 Ponded condition.

Figure 7. Appearance of the models at 10 seconds after the start of the experiments.

resistance due to water immersion, as discussed in Chapter 3. It is presumed that the formation of a water level generated pore water pressure, which reduced shear strength and thus increased erosion.

5.2 *Influence of the Degree of Saturation on the Degree of Erosion*

The assumed water level at the end of the rainfall simulation in Case 4 is shown in Figure 6(b). While the converted water levels based on measurements from sensors PWP06 and PWP07 exceeded the slope height, this is likely due to pore water pressure resulting from discharge from the slope toe. Although the water level immediately before the overflow test was not measured, a 150-minute resting period was provided after the rainfall test, and it is presumed that the water level had decreased from the level at the end of rainfall.

The erosion conditions at 10 seconds after the start of the experiments for Cases 3 and 4 are shown in Figure 9, and cross-sectional sketches at the glass surface are presented in Figure 10. No significant differences were observed between the model cross sections at 10 and 20 seconds after the start of the experiments.

In Case 3, the degree of saturation measured by sensors M01 to M03 at the start of the overflow test ranged from 50.1% to 55.9%, while in Case 4, the degree of saturation measured by M01 to M04 ranged from 63.5% to 76.5%. Although the water level was distributed at lower positions in Case 4, and the effect was considered limited, the difference in erosion volume compared to Case 3 under higher the degree of saturation conditions was minimal.

From these results, it can be concluded that under conditions of water level, changes in the degree of saturation have little effect on erosion volume. Compared to the influence of pore water pressure, the effect of the degree of saturation alone on erosion resistance characteristics is considered minor.

6 CONCLUSION

In this study, an experimental investigation was conducted to evaluate the effects of soil moisture conditions on the erosion resistance of embankment materials, with the aim of establishing a method for assessing erosion failure on embankment slopes. Based on the results of the erosion tests and model overflow experiments, the following findings were obtained:

1. The results of erosion tests with varying initial water contents showed that under low flow velocity conditions, the effect of initial water content on erosion resistance was limited. In contrast, specimens with lower initial water content exhibited higher erosion resistance under high flow velocity conditions. Observations of erosion patterns revealed that under low flow velocities, soil particle detachment was dominant, suggesting that erosion resistance is governed primarily by the weight of individual particles. Under high flow velocities, however, the detachment of soil clods was more prevalent, indicating that the erosion resistance is mainly governed by the shear strength of the specimens.

   In the erosion tests, specimens subjected to water immersion showed a greater reduction in erosion resistance under high flow velocity conditions compared to non-immersed specimens. It is inferred that water immersion caused the development of pore water pressure, leading to a decrease in effective stress and, consequently, a reduction in shear strength and erosion resistance. This trend was particularly evident in specimens with initial water content at or above the optimum level.

2. Specimens with low initial water content exhibited relatively low erosion resistance regardless of water immersion. This is likely because lower initial water content allowed for higher infiltration, resulting in a moisture condition comparable to that of immersed specimens, and thus similar erosion resistance.
2. The model overflow experiments demonstrated that a higher water level in the embankment significantly increased erosion. On the other hand, under conditions of low water levels—where the influence of pore water pressure was limited—changes in the degree of saturation had little effect on the degree of erosion.

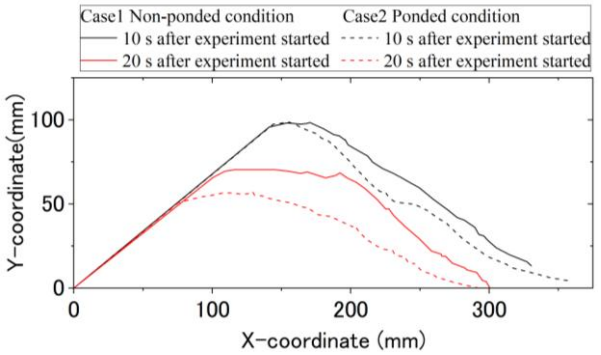

Figure 8. Sketches of the external appearance of the models during overflow experiments with and without ponding water.

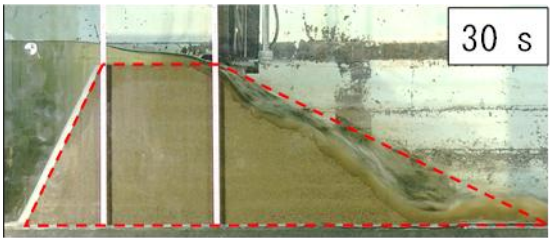

(a) Case 3 Non-rainfall condition.

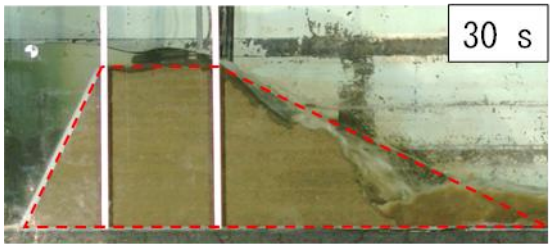

(b) Case 4 Rainfall condition.

Figure 9. Appearance of the models at 30 seconds after the start of the experiments.

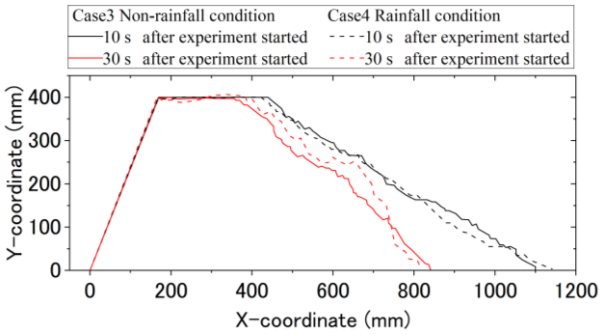

Figure 10. Sketches of the external appearance of the model during overflow experiments with and without rainfall.

7 REFERENCES

Briaud, J, L., Ting, F. C., Chen, H, C., Gundavalli, R., Perugu, S. and Wei, G. 1999. Prediction of scour rate in cohesive soils at bridge piers. *Journal of Geotechnical and Geoenvironmental Engineering* 125(4), 237-246.

Fujisawa, K., Kobayashi, A. and Yamamoto, K. 2008. Erosion rates of compacted soils for embankmen., *Journal of JSCE C* 64(2), 403-410.

Mizutani, H., Nakagawa, H., Yoden, T., Kawaike, K., & Zhang, H. 2013. Numerical modelling of river embankment failure due to overtopping flow considering infiltration effects. *Journal of Hydraulic Research* 51(6), 681-695.

Nishimori, K. and Sekine, M. 2009. Erosion rate formula of cohesive sediment. *Japanese Journal of JSCE* 65(2), 127-140. (in Japanese)

Philip, J, R. 1969. Theory of infiltration. *Advances in hydroscience* 5, 215-296.

Watanabe, K., Nakajima, S., Fujii, K., Matsuura, K., Kudo, A., Nonaka, T. and Aoyagi, Y. 2020. Development of geosynthetic-reinforced soil embankment resistant to severe earthquakes and prolonged overflows due to tsunamis. *Soil and Foundations* 60, 1371-1386.

Wei, L., Yang, M., Shao, J., Li, L., Chen, P., Li, S. and Zhao, R. 2022. Experimental investigation of relationship between infiltration rate and soil Moisture under rainfall conditions. *Water* 14(9), 1347.